Chemical Science

ROYAL SOCIETY OF CHEMISTRY

EDGE ARTICLE

View Article Online
View Journal | View Issue

Check for updates

Cite this: *Chem. Sci.*, 2023, **14**, 9943

All publication charges for this article have been paid for by the Royal Society of Chemistry

Received 8th June 2023
Accepted 30th August 2023

DOI: 10.1039/d3sc02943c

rsc.li/chemical-science

An artificial light-harvesting system constructed from a water-soluble metal–organic barrel for photocatalytic aerobic reactions in aqueous media†

Danyang Li,[a] Linlin Yang,[b] Wangjian Fang,[c] Xinmei Fu,[a] Hechuan Li,[a] Jianxu Li,[a] Xuezhao Li[a] and Cheng He*[a]

An artificial light-harvesting system constructed from a water-soluble host–guest complex can be regarded as a high-level conceptual model of its biological counterpart and can convert solar energy into chemical energy in an aqueous environment. Herein, a water-soluble metal–organic barrel **Ga-tpe** with twelve sulfonic acid units was obtained by subcomponent self-assembly between Ga^{3+} ions and tetra-topic ligands with tetraphenylethylene (TPE) cores. By taking advantage of host–guest interactions, cationic dye rhodamine B (**RB**) was constrained in the pocket of **Ga-tpe** to promote the Förster resonance energy transfer (FRET) process for efficient photocatalytic aerobic oxidation of sulfides and cross-dehydrogenative coupling (CDC) reaction in aqueous media.

Introduction

The construction of molecular containers has provided a sustainable way to mimic and rival natural organisms and enzymes.[1] Among such cage-like hosts, the coordination-driven assembly of metal–organic cages, which can be functionalized with both organic ligands and metal centers, has been considered an excellent candidate to mimic enzymes, due to their precisely controlled, well-defined topology obtained using facile synthesis and stability in common solvents.[2,3] With highly selective recognition toward substrates inside their large inner cavity, such discrete coordination constructs have proven useful as molecular devices for substrate encapsulation,[4] separation,[5] and reaction vessels to catalytically accelerate chemical processes.[6,7]

Specifically, supramolecular assemblies formed by cage hosts and encapsulated guests with essential components being forced into close proximity have also attracted constant attention to developing supramolecular charge/energy donor–acceptor systems, which led to efficiency enhancements in energy, electron, or substance transfers based on short through-space and long through-bond pathways.[8,9] For example, inspired by nature, significant advances have been made in using supramolecular donor–acceptor systems to mimic light antenna harvesting systems using the FRET process.[10–14] Previously, we reported a highly efficient supramolecular FRET system using a large metal–organic cage as a donor. It was thought that encapsulation of the guest within the inner cavity of the cage would render the interaction between the donor and the acceptor stronger and more robust in close proximity and the rigid coordination cage could provide an isolated microenvironment in which the donors could be fixed at a high local concentration without further aggregation.[15]

It is nearly universal in natural systems that most host–guest interactions based on biological processes are executed under aqueous conditions.[16] Nevertheless, most metal–organic cages have been prepared and studied in organic solvents. It is appealing to create water-soluble metal–organic cages that could be regarded as high-level conceptual models for their biological counterparts.[17] Water-soluble metal–organic cages with large inner pockets have found widespread use in the selective storage and transport of a variety of guest molecules, as well as in the promotion of chemical reactions.[18–20] To achieve this goal, the design of water-soluble and stable metal–organic cages is highly desired but has been challenging due to the following: first, these discrete coordination structures need to maintain rigidity and stability, which requires the ligands to contain nonpolar aromatic backbones; however, in this case, the aromatic ligand is poorly soluble in aqueous solutions. Second, due to the coordinating ability of water, it can bind to metal centers, compete with ligands, and reduce the formation of metal–organic cages. Third, hydrophobic effects may change the way ligands organize around metal ions, leading to aggregation as opposed to the formation of hollow cages.

[a]*State Key Laboratory of Fine Chemicals, Dalian University of Technology, Dalian 116012, P. R. China. E-mail: hecheng@dlut.edu.cn*

[b]*Xinxiang Key Laboratory of Forensic Science Evidence, School of Forensic Medicine, Xinxiang Medical University, Xinxiang 453003, P. R. China*

[c]*Institute for Molecular Design and Synthesis, School of Pharmaceutical Science & Technology, Tianjin University, Tianjin 300072, P. R. China*

† Electronic supplementary information (ESI) available. See DOI: https://doi.org/10.1039/d3sc02943c

Open Access Article. Published on 31 August 2023. Downloaded on 1/18/2026 3:45:56 PM. This article is licensed under a Creative Commons Attribution-NonCommercial 3.0 Unported Licence.

Open Access Article. Published on 31 August 2023. Downloaded on 1/18/2026 3:45:56 PM.
This article is licensed under a Creative Commons Attribution-NonCommercial 3.0 Unported Licence.

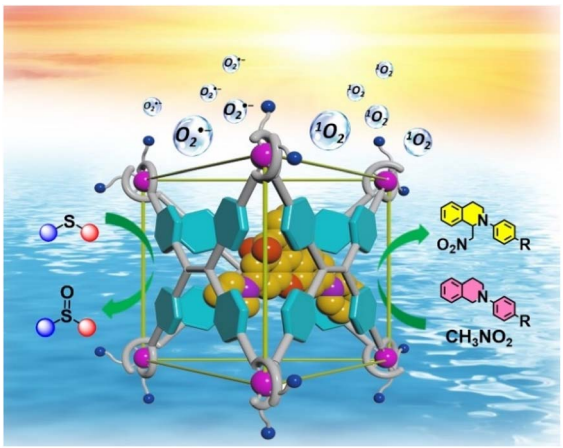

Scheme 1 The illustration of the host–guest strategy between **Ga-tpe** and the encapsulated **RB** dye in inducing effective FRET processes for highly efficient photocatalytic aerobic reactions.

Thus, to better imitate natural light-harvesting antenna systems, establishing supramolecular FRET systems in aqueous environments to convert solar energy into chemical energy is of great significance. Herein, an anionic metal–organic barrel **Ga-tpe** endowed with water solubility was constructed using subcomponent self-assembly for application as an energy donor. **Ga-tpe** was capable of encapsulating the positively charged guest **RB** as a suitable energy acceptor. It was envisioned that a FRET process in an aqueous environment could be enabled between the face-capped cage **Ga-tpe** and the **RB** dye with a high local donor–acceptor ratio and minimized distance between them. Significantly, the harvested solar energy could be utilized to promote the photooxidation of thioanisole and photocatalyzed aerobic CDC reactions in an aqueous medium. Thus, the **RB@Ga-tpe** supramolecular system could be regarded as a promising natural counterpart to initiate photocatalytic reactions in a simulated enzymatic environment (Scheme 1).

Results and discussion

Synthesis and characterization of cage Ga-tpe

Ga-tpe was formed by the reaction of 4,4′,4″,4‴-(ethene-1,1,2,2-tetrayl)tetra(benzohydrazide) (3 equiv.), 5-sulfosalicylaldehyde sodium salt (12 equiv.), gallium tris(acetylacetonate) (6 equiv.) and NaOH (24 equiv.) in methanol at 60 °C overnight (Fig. 1a). The ^{1}H NMR spectra of **Ga-tpe** with a single set of ligand environments were recorded in D_2O, and the broad signals of **Ga-tpe** were indicative of the formation of the cage structure (Fig. S7, ESI†). Moreover, the ^{1}H diffusion-ordered (DOSY) NMR spectrum of **Ga-tpe** showed the formation of a single species with a diffusion coefficient (D) value of 3.47×10^{-11} m^2 s^{-1} (Fig. 1b). Thanks to the twelve sulfonic acid units of the cage **Ga-tpe**, the water solubility and stability of the cage were realized (Fig. S9, ESI†).

Electrospray ionization mass spectrometry (ESI-MS) of **Ga-tpe** showed a set of signals at m/z = 561.6986, 645.2128, 756.5973, confirming the formation of a Ga_6L_3 metal–organic barrel (Fig. 1c). A simple comparison with the simulation results based on natural isotopic abundances suggested that the peaks corresponded to a characteristic sequence of signals associated with the loss of different numbers of cations, $[Ga_6L_3 \cdot n(Na^+)H]^{(17-n)-}$ (n = 9–11).

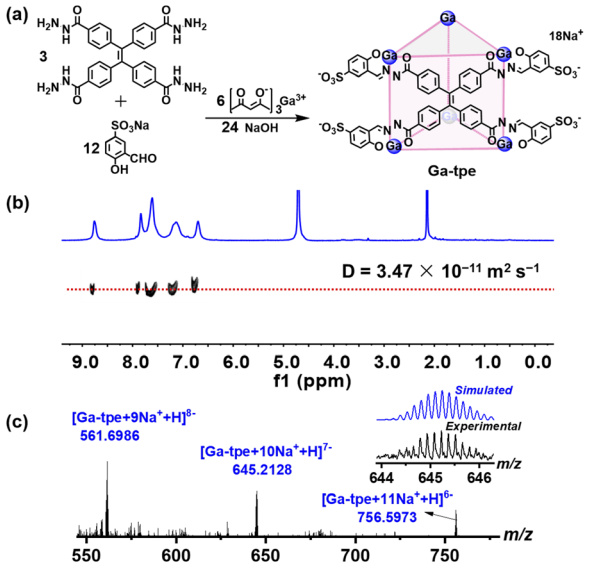

Fig. 1 (a) The self-assembly of **Ga-tpe**; (b) DOSY spectrum of **Ga-tpe** in D_2O; (c) the ESI-MS spectra of **Ga-tpe**.

Unfortunately, several trials were conducted to obtain a single crystal of **Ga-tpe** but were unsuccessful. The structural optimization calculation was employed,[21] providing a clear picture of the structural pattern of **Ga-tpe** (Fig. 2). The optimized structure of **Ga-tpe** revealed the formation of a Ga_6L_3 barrel consisting of three TPE ligands and six gallium ions. There was the possibility of the formation of two isomeric barrels where the ligand panels could be horizontally oriented (Fig. 2a–c) or vertically oriented (Fig. 2e–f). Hence, the six Ga

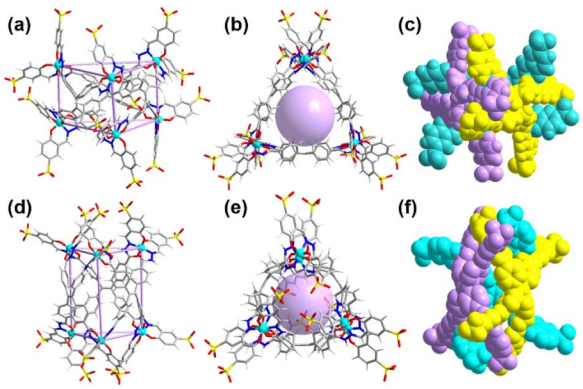

Fig. 2 Optimized structure of barrel **Ga-tpe**. (a) and (b) The different views where ligands were horizontally oriented; (c) the filling pattern of **Ga-tpe**; (d) and (e) the different views of the other expected geometry where ligands were vertically oriented; (f) the filling pattern of **Ga-tpe**. Color codes: Ga turquoise, N blue, S yellow, O red, C grey, and H white.

© 2023 The Author(s). Published by the Royal Society of Chemistry

Open Access Article. Published on 31 August 2023. Downloaded on 1/18/2026 3:45:56 PM. This article is licensed under a Creative Commons Attribution-NonCommercial 3.0 Unported Licence.

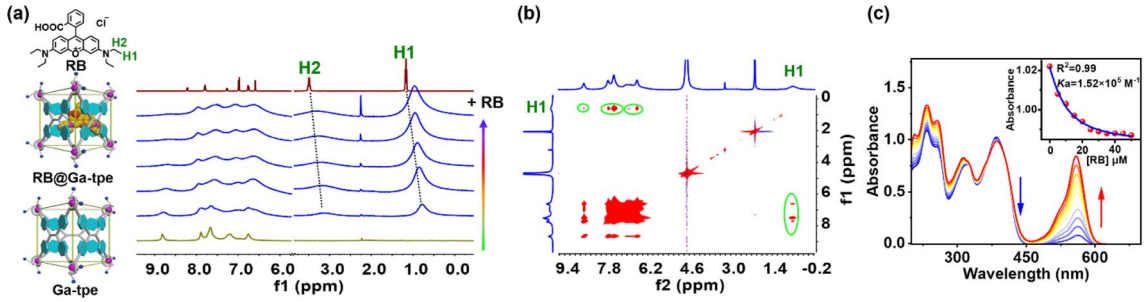

Fig. 3 (a) The ^{1}H NMR titration spectra between **Ga-tpe** ([**Ga-tpe**] = 2.0×10^{-3} M) and **RB** (1 equiv. per session) in D_2O; (b) the NOESY spectrum of **Ga-tpe** with **RB** in D_2O; (c) the absorbance spectra of **Ga-tpe** ([**Ga-tpe**] = 1.0×10^{-5} M) upon the addition of **RB** in water. Inset: nonlinear fitting of the titration curve at 385 nm, showing the calculated associate constant $K_a = 1.52 \times 10^5$ M^{-1}.

ions were located at the vertices of the barrel, whereas the three ligands served as the three faces of the barrel to form a pocket for the recognition and localization of guests (such as **RB** or **MB**) in the host. Moreover, the results suggested that coordination-driven restricted rotation of the TPE-ligand would prohibit nonradiative decay.[22]

Host–guest complex with encapsulated RB

Driven by possible aromatic interactions, H bond interactions, and electrostatic interactions in the **Ga-tpe** pocket, the cationic energy acceptor **RB** with a suitable size was expected to be encapsulated in the **Ga-tpe** cage as a guest, not only avoiding the aggregation-caused quenching effect of the aggregated dye but also forcing close proximity between the energy donor and acceptor to meet the need for a highly efficient FRET process. The mode of interaction between **Ga-tpe** and **RB** was studied by isothermal titration calorimetry assays, and the combined number indicated that the presence of **RB** triggered the formation of an **RB@Ga-tpe** 1 : 1 host–dye complex in water (Fig. S10, ESI†). Curve fitting by computer simulation using an "independent" model showed an association constant of 1.22×10^5 M^{-1}.

The formation of the host–guest complex was further evidenced by the ^{1}H NMR titration experiment between metal–organic barrel **Ga-tpe** and **RB** (Fig. 3a). The addition of **RB** to **Ga-tpe** showed significant upfield shifts (0.42 ppm and 0.38 ppm) where the methyl (H1 and $-CH_3$) and the methylene (H2 and $-CH_2-$) protons of **RB** were observed. Furthermore, H–H interactions between the aromatic rings, –NH– of **Ga-tpe** and methyl (H1) protons of **RB** could be observed in the nuclear Overhauser effect (NOESY) spectrum of **RB@Ga-tpe** (Fig. 3b), which showed the guest **RB** to reside within the pocket of **Ga-tpe** and the donor host and acceptor guest were close enough in space for efficient energy transfer. The binding constant of **RB** with **Ga-tpe** was detected by UV-Vis titration in water and nonlinear fitting of the titration curve with an association constant ($K_a = 1.52 \times 10^5$ M^{-1}) (Fig. 3c). With a gradually increasing ratio of **RB** to **Ga-tpe**, the absorption peak of **Ga-tpe** at 385 nm gradually decreased, causing significant variation in these bands with sharp isosbestic points at 360 nm and 415 nm, suggesting the formation of a host–guest complex between **Ga-tpe** and **RB**.

Artificial light harvesting by Förster resonance energy transfer

The effective FRET process requires not only an appropriate distance and dipole orientation between different chromophores but also a match in the spectral overlap between the donor emission and acceptor excitation. **RB** was chosen as an energy acceptor because of the good overlap between the fluorescence band of **Ga-tpe** and the absorption spectra of **RB** (Fig. 4a). The FRET process was shown by fluorescence titration of **RB** with the aqueous solution of **Ga-tpe** (Fig. 4b). Interestingly, with an increasing concentration of **RB** in **Ga-tpe**, the broad emission peak of **Ga-tpe** at 505 nm was gradually decreased, while a new emission peak of **RB@Ga-tpe** at 590 nm appeared when excited at 385 nm. Moreover, the CIE chromaticity diagram confirmed the obvious fluorescence color change from blue to pink under UV light (Fig. 4c). Alternatively, the addition of **Ga-tpe** to the solution of **RB** showed that the intensity of **Ga-tpe** and **RB** gradually increased when excited at 385 nm, revealing the highly efficient energy transfer from **Ga-tpe** to **RB** (Fig. 4d).

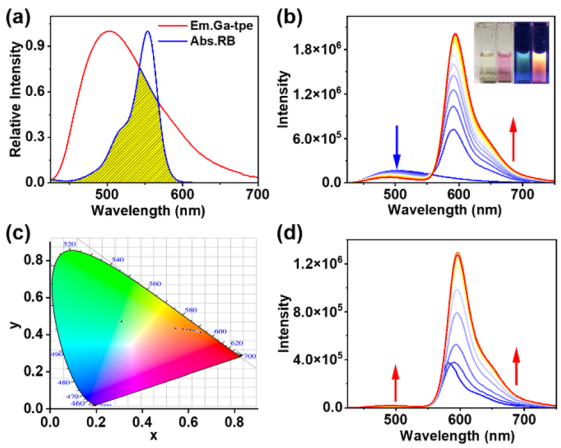

Fig. 4 (a) Normalized fluorescence spectrum of **Ga-tpe** and the absorbance spectrum of RB; (b) fluorescence spectrum of **Ga-tpe** ([**Ga-tpe**] = 1.0×10^{-5} M) in water with different concentrations of RB (0.05 equiv. per session); (c) the CIE chromaticity diagram changes of **Ga-tpe** upon titration with RB; (d) fluorescence spectrum of RB ([RB] = 1.0×10^{-5} M) in water with different concentrations of **Ga-tpe**.

© 2023 The Author(s). Published by the Royal Society of Chemistry

Open Access Article. Published on 31 August 2023. Downloaded on 1/18/2026 3:45:56 PM. This article is licensed under a Creative Commons Attribution-NonCommercial 3.0 Unported Licence.

Compared to that of **Ga-tpe** (1.37%), the quantum yield of **RB@Ga-tpe** increased to 15.76%, which further confirmed the occurrence of the FRET process (Fig. S12, Table S1 ESI†). In addition, the fluorescence lifetime of **Ga-tpe** followed a double exponential decay, which showed $\tau_{int} = 1.04$ ns when emitting at 405 nm (Fig. S13, Table S2 ESI†). In contrast, the fluorescence lifetime of **RB@Ga-tpe** was found to be shorter in the presence of **RB** (τ_{int} = 0.98 ns), which suggested that energy could be transferred from the donor **Ga-tpe** to the acceptor **RB**. As a result, the Φ_{ET} of **RB@Ga-tpe** reached 56.1% (ESI, Table S3†).

In addition, the importance of host–guest interaction in the FRET system was identified by preventing the FRET process by binding an inhibition guest in the pocket of **Ga-tpe**. Methylene blue 2B (**MB**) is a cationic dye similar to **RB**, which is smaller than **RB**. **MB** was chosen as a competitive guest introduced into the host–guest system. The fluorescence and UV-Vis absorption titration indicated that **MB** was a suitable competitive guest for binding into the pocket of **Ga-tpe** to replace **RB** (Fig. S14, ESI†). Notably, upon the gradual addition of **MB** to the mature **RB@Ga-tpe** FRET system, the emission peak of the system at 590 nm gradually decreased (Fig. S15, ESI†). This showed that **MB** competed with **RB** for binding into **Ga-tpe** to inhibit the FRET process, resulting in a decrease in the emission intensity of **RB@Ga-tpe**. The effect of the host–guest interaction on the FRET processes was also identified using the fluorescence titration of **RB** with a solution of ligand **L**. Even though the absorption of **RB** overlapped well with the emission of **L**, the broad emission peak of ligand **L** at 520 nm slightly decreased upon the gradual addition of **RB** to a solution of ligand **L** (Fig. S16, ESI†).

Research on reactive oxygen species (ROS)

To better display the versatility of **RB@Ga-tpe**, we explored its use in photocatalytic oxidation reactions. Subsequently, we investigated the capacity of **RB@Ga-tpe** to generate ROS using 3,3′,5,5′-tetramethylbenzidine (TMB) as a probe molecule. Upon adding **RB@Ga-tpe** into a methanol solution containing TMB, the characteristic absorption peak of the oxidized TMB at around 670 nm increased significantly with Xe light irradiation time in an air atmosphere (Fig. 5a), suggesting the formation of ROS. For comparison, the absorption became lower under similar conditions when performed with **Ga-tpe** or **RB** only (Fig. 5b and S18, ESI†), respectively, indicating that the artificial light-harvesting system benefitted oxygen activation.

To clarify the various types of ROS that were generated when using **RB@Ga-tpe**, the electron paramagnetic resonance (EPR) spectra using 2,2,6,6-tetramethylpiperidine (TEMP) and 5,5-dimethyl-1-pyrroline *N*-oxide (DMPO) as ROS trapping agents were recorded under xenon lamp irradiation and in an air-saturated CH_3OH solution (Fig. 5c and d). The obvious characteristics of singlet oxygen ($^1O_2$) and superoxide ($O_2^{\bullet-}$) were trapped. The results showed that the active oxygen species $^1O_2$ and $O_2^{\bullet-}$ could be produced by using **RB@Ga-tpe** as a photocatalyst, generated by an energy transfer process and single electron transfer.

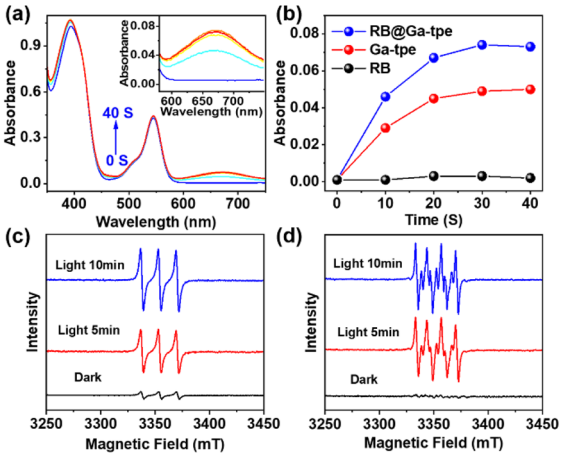

Fig. 5 (a) Evolution of the UV-Vis spectra during the continuous irradiation of **RB@Ga-tpe** with Xe light in the presence of TMB in an air atmosphere; (b) time-dependent corresponding absorption of TMB at 670 nm; (c) the detection of $^1O_2$ in a mixture of TEMP and **RB@Ga-tpe** in methanol solution under xenon lamp irradiation using EPR spectra in an air atmosphere; (d) the detection of $O_2^{\bullet-}$ in a mixture of DMPO and **RB@Ga-tpe** in methanol solution under xenon lamp irradiation using EPR spectra in an air atmosphere.

Photooxidation of sulfides to sulfoxides

To use the output energy to simulate the natural photosynthetic process, the above artificial light-harvesting system based on **RB@Ga-tpe** was applied as a photocatalyst for the oxidation of thioanisole in water (Table 1). As expected, an excellent yield (90%) and selectivity capability (>99%) on the sulfide being transformed into sulfoxide have been achieved in an aqueous

Table 1 Photooxidation of sulfide to sulfoxide[a]

Entry	Photocatalyst	Light	Conv. (%)	Selectivity (%) 1a	1b
1	**RB@Ga-tpe**	Xe	90	>99	<1
2	**RB**	Xe	13	>99	<1
3	**Ga-tpe**	Xe	n.d.	0	0
4	**L**	Xe	10	>99	<1
5	**L&RB**	Xe	30	>99	<1
6	Blank	Xe	n.d.	0	0
7[b]	**RB@Ga-tpe**	Xe	n.d.	0	0
8	**RB@Ga-tpe**	Dark	n.d.	0	0
9	**Ga-tpe**	395 nm	23	>99	<1
10	**RB**	395 nm	n.d.	0	0
11	**RB@Ga-tpe**	395 nm	55	>99	<1

[a] Reaction conditions, thioanisole (0.2 mmol, 1 equiv.), catalyst (0.5 mol%), water (2 ml), room temperature, 12 h, air. [b] Ar. The yields were determined by GC analysis (using 1,3,5-trimethoxybenzene as the internal standard).

© 2023 The Author(s). Published by the Royal Society of Chemistry

Open Access Article. Published on 31 August 2023. Downloaded on 1/18/2026 3:45:56 PM. This article is licensed under a Creative Commons Attribution-NonCommercial 3.0 Unported Licence.

solution and when irradiated with a Xe light (Table 1, entry 1). Exhilaratingly, the yield of **1a** increased dramatically upon using the light-harvesting system **RB@Ga-tpe** compared with using either **RB** or **Ga-tpe** only (Table 1, entries 2 and 3). Meanwhile, the control experiments using ligand **L** or **L&RB** yielded a trace of the product under the same conditions, confirming that the supramolecular host using the preorganization of an artificial light-harvesting system is essential (Table 1, entries 4 and 5). Furthermore, a series of control experiments were carried out to confirm that the presence of light, photosensitizer, and O_2 is essential for the catalytic reaction under similar conditions (Table 1, entries 6–8). Then, 395 nm light (the near absorption of **Ga-tpe**) triggered the photocatalytic reaction, the slightly high yield (**RB@Ga-tpe** as the photocatalyst) was 55%, and the lower yield (**Ga-tpe** or **RB** as the photocatalyst) was obtained (Table 1, entries 9–11). The results indicated that the photooxidation reaction could also use 395 nm light through the absorption of **Ga-tpe**, expanding the range of the catalytic light source.

Encouraged by the remarkable photocatalytic performance, the substrate compatibility of **RB@Ga-tpe** with various sulfides was further explored. As shown in Table S4,† **RB@Ga-tpe** exhibited excellent activity and selectivity toward other methylphenyl sulfide derivatives with different substituents, such as methoxy (–OMe) and fluorine (–F). Due to the limited solubility of the substrate in aqueous solution, when a small amount of methanol was added to the system, the yield of sulfoxides (**1e–i**) was significantly improved. In the photooxidation of sulfides, a series of quenching experiments were carried out by introducing various scavengers, such as sodium azide (NaN_3, a scavenger of $^1O_2$), 1,4-benzoquinone (BQ, a scavenger of $O_2^{\bullet-}$), isopropanol (IPA, a scavenger of $^{\bullet}OH$), and $AgNO_3$ (as an electron trapping agent), respectively. The photooxidation reactions were effectively prohibited by adding sodium azide and BQ, whereas other scavengers exerted less influence than them, which revealed that $^1O_2$ and $O_2^{\bullet-}$ should be the dominant reactive species (Fig. S19a and S20, ESI†).[23]

Photocatalytic aerobic CDC reaction

The **RB@Ga-tpe** assembly with catalytic efficiency for the oxidation of sulfides was then expanded to other photocatalytic oxidative organic transformations, such as photocatalytic aerobic CDC reactions (Table 2), a highly efficient and powerful strategy for the construction of new carbon–carbon and carbon–heteroatom bonds, which has been considered a waste-minimized and sustainable synthetic alternative to classic coupling procedures.[24] In particular, the photocatalytic C–H functionalization of tertiary amines is the most atom-economic and sustainable reaction process. The aerobic CDC reaction of *N*-phenyl-1,2,3,4-tetrahydroisoquinoline **2a** and nitromethane with **RB@Ga-tpe** as a photocatalyst was selected as a model photocatalytic reaction. The blank reaction was performed under the same conditions, and a moderate yield was shown (50%, Table 2, entry 5). Alone, **Ga-tpe**, **RB**, or **L**, as the photocatalyst, produced relatively low yields in aqueous solution (52–65%, Table 2, entries 2–4). For comparison, the activity of

Table 2 Photocatalytic aerobic CDC reaction[a]

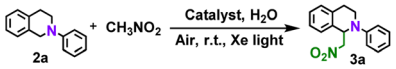

Entry	Photocatalyst	Light	Yield rate (%)
1	**RB@Ga-tpe**	Xe	90
2	**Ga-tpe**	Xe	65
3	**RB**	Xe	59
4	**L**	Xe	52
5	Blank	Xe	50
6	**RB@Ga-tpe**	Dark	n.d.
7	**L&RB**	Xe	70
8	**Ga-tpe**	395 nm	34
9	**RB**	395 nm	25
10	**RB@Ga-tpe**	395 nm	51

[a] Reaction conditions: *N*-phenyl-1,2,3,4-tetrahydroisoquinoline (0.1 mmol, 1 equiv.), nitromethane (0.3 ml), catalyst (1.0 mol%), water solution (2 ml), room temperature, 12 h. The yields were determined by ^1H NMR analysis using 1,3,5-trimethoxybenzene as an internal standard.

RB@Ga-tpe in the photocatalytic CDC reaction was investigated; an excellent yield of 90% was achieved under the same conditions (Table 2, entry 1). However, a moderate reaction yield was obtained by the assembly resembling **L&RB** (70%, Table 2, entry 7). These above results revealed that light energy harvested using **Ga-tpe** could be efficiently transferred to **RB** within the host–guest encapsulated system, and the **RB@Ga-tpe** system could be an ideal reaction platform for organic reactions in aqueous solutions.

A series of quenching experiments were also carried out by introducing various scavengers into the CDC reaction (Fig. S19b, ESI†). Unsurprisingly, the abovementioned studies demonstrated that the superoxide radical anion is the active intermediate in the photocatalytic CDC reactions. According to the above findings and literature results,[25] the photocatalytic CDC reaction mechanism between *N*-phenyl-1,2,3,4-tetrahydroisoquinoline and nitromethane was proposed (Fig. S21, ESI†). The **RB@Ga-tpe** assembly was excited using Xe light in an aqueous solution, and the excited state of **Ga-tpe** transferred the energy to the acceptor dye **RB** to form the excited state of **RB**. As shown in Table 3, we further explored the substrate scope; generally, *N*-phenyl-1,2,3,4-tetrahydroisoquinoline derivatives with different electronic properties could be converted to the desired reaction products **3a–h** in excellent yields (71–94%).

Overall, these results confirmed that the photocatalytic aerobic reaction was initiated by the supramolecular assembly in the aqueous phase, and dye-loaded capsule **RB@Ga-tpe** could be regarded as one kind of biological counterpart. The host–guest species **RB@Ga-tpe** with excellent photocatalytic ability can serve as an efficient light-harvesting system where the output energy was successfully utilized for catalytic chemical transformation for practical application in the aqueous phase. The reason why the dye-loaded capsule **RB@Ga-tpe** exhibited

Open Access Article. Published on 31 August 2023. Downloaded on 1/18/2026 3:45:56 PM. This article is licensed under a Creative Commons Attribution-NonCommercial 3.0 Unported Licence.

Table 3 The substrate scope of the CDC reaction[a]

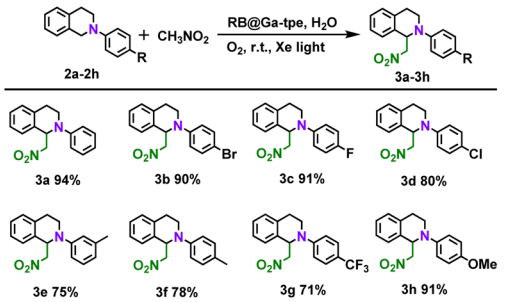

[a] Reaction conditions: *N*-phenyl-1,2,3,4-tetrahydroisoquinoline derivative (0.1 mmol, 1 equiv.), nitromethane (0.3 ml). **RB@Ga-tpe** assembly solution (**RB : Ga-tpe** = 1 : 1, 1.0 mol%, 2 ml), Xe light, oxygen ball, room temperature, 18 h. The yields were determined by ^{1}H NMR analysis using 1,3,5-trimethoxybenzene as an internal standard.

high catalytic efficiency might be that the host–guest arrangement between the cage **Ga-tpe** and **RB** in a confined space avoids unnecessary fluorescence quenching, and the photobleaching effect of **RB** upon long-time irradiation was also decreased because of the formation of a supramolecular assembly. Thus, we believe that such an efficient host–guest system with an energy transfer process would provide new insight into the fabrication of artificial photosynthetic systems.

Conclusions

In summary, a new negatively charged metal–organic barrel **Ga-tpe** endowed with water solubility was reported for the construction of a light-harvesting system by host–guest interactions to accelerate light-driven aerobic reactions in aqueous media. The energy acceptor **RB** was matched to generate the FRET process by rendering the host–guest interaction between the donor and the acceptor stronger and more robust in close proximity. The artificial light-harvesting system **RB@Ga-tpe** had suitable potential for the photooxidation of sulfides to sulfoxides reaction and photocatalytic CDC reactions in simulating the photosynthesis process. Overall, this work presents an ideal way for the creation of a water-soluble artificial light-harvesting system *via* host–guest encapsulation to enhance the efficiency of the FRET process, serving as a versatile platform for mimicking natural photosynthesis in a simulated enzymatic environment. The further development of metal–organic host–guest assemblies in aqueous solutions that mimic natural organisms will be facilitated and accelerated in the future.

Experimental

Preparation of Ga-tpe

A mixture of 4,4′,4″,4‴-(ethene-1,1,2,2-tetrayl)tetra (benzohydrazide) (84.7 mg, 0.15 mmol), 5-sulfosalicylaldehyde sodium salt (134.8 mg, 0.6 mmol), NaOH (48 mg, 1.2 mmol), and gallium tris(acetylacetonate) (110.1 mg, 0.3 mmol) was dissolved in 30 mL CH_3OH and then heated at 60 °C for 24 h to give a clear yellow solution. The mixture was repeatedly recrystallized from dichloromethane and acetone to afford a yellow solid with 65.6% yield (based on the solid dried under vacuum). ^{1}H NMR (400 MHz, D_2O) δ 8.76 (s, 4H), 7.84 (s, 4H), 7.61 (s, 12H), 7.13 (s, 8H), 6.70 (s, 4H). ^{13}C NMR (100 MHz, MeOD) δ 193.78, 180.44, 170.44, 168.75, 161.46, 156.96, 147.08, 134.59, 133.11, 132.02, 128.35, 122.01, 118.21.

General procedure for the RB@Ga-tpe photocatalytic oxidation of thioanisole

Thioanisole (0.2 mmol, 1 equiv.), catalyst (0.5 mol%), and H_2O (2 ml) were added to a glass reactor and irradiated with a Xe lamp at room temperature for 12 h in an air atmosphere. At the end of the reaction, it was extracted using dichloromethane. The yields were monitored using gas chromatography (GC) and ^{1}H NMR analysis relative to the internal standard 1,3,5-trimethoxybenzene.

General procedure for the RB@Ga-tpe photocatalytic aerobic CDC reaction

N-Phenyl-1,2,3,4-tetrahydroisoquinoline (0.1 mmol, 1 equiv.), nitromethane (0.3 ml), catalyst (1.0 mol%), and H_2O (2 ml) were added to a glass reactor and irradiated using a Xe lamp at room temperature for 12 h in an air atmosphere. After the indicated time, it was extracted using ethyl acetate and concentrated under vacuum distillation. The yields were determined by ^{1}H NMR analysis using 1,3,5-trimethoxybenzene as an internal standard.

Data availability

All the data supporting this article have been included in the main text and the ESI.†

Author contributions

C. He and D. Li designed the research and co-wrote the manuscript. D. Li, H. Li, and J. Li performed all experiments. W. Fang carried out structural optimization calculations. X. Fu performed ESI-MS. L. Yang and X. Li assisted in analyzing the data.

Conflicts of interest

There are no conflicts to declare.

Acknowledgements

This work was supported by the National Natural Science Foundation of China 22171033 and the Fundamental Research Funds for the Central Universities [DUT17RC(3)094].

Notes and references

1 (*a*) T. R. Cook, Y.-R. Zheng and P. J. Stang, *Chem. Rev.*, 2013, **113**, 734–777; (*b*) T. R. Cook and P. J. Stang, *Chem. Rev.*, 2015,

© 2023 The Author(s). Published by the Royal Society of Chemistry

Open Access Article. Published on 31 August 2023. Downloaded on 1/18/2026 3:45:56 PM. This article is licensed under a Creative Commons Attribution-NonCommercial 3.0 Unported Licence.

115, 7001–7045; (*c*) D. Zhang, T. K. Ronson and J. R. Nitschke, *Acc. Chem. Res.*, 2018, **51**, 2423–2436.

2 (*a*) Y. Tamura, H. Takezawa and M. Fujita, *J. Am. Chem. Soc.*, 2020, **142**, 5504–5508; (*b*) M. D. Ludden, C. G. P. Taylor and M. D. Ward, *Chem. Sci.*, 2021, **12**, 12640–12650; (*c*) S. Hasegawa, S. L. Meichsner, J. J. Holstein, A. Baksi, M. Kasanmascheff and G. H. Clever, *J. Am. Chem. Soc.*, 2021, **143**, 9718–9723; (*d*) M. Ueda, N. Kishida, L. Catti and M. Yoshizawa, *Chem. Sci.*, 2022, **13**, 8642–8648; (*e*) L. R. Holloway, P. M. Bogie, Y. Lyon, C. Ngai, T. F. Miller, R. R. Julian and R. J. Hooley, *J. Am. Chem. Soc.*, 2018, **140**, 8078–8081; (*f*) R. Banerjee, D. Chakraborty and P. S. Mukherjee, *J. Am. Chem. Soc.*, 2023, **145**, 7692–7711.

3 (*a*) W.-X. Gao, H.-N. Zhang and G.-X. Jin, *Coord. Chem. Rev.*, 2019, **386**, 69–84; (*b*) X.-X. Gou, T. Liu, Y.-Y. Wang and Y.-F. Han, *Angew. Chem., Int. Ed.*, 2020, **59**, 16683–16689; (*c*) H. Wang, Y. Li, N. Li, A. Filosa and X. Li, *Nat. Rev. Mater.*, 2021, **6**, 145–167; (*d*) Y. Hou, Z. Zhang, S. Lu, J. Yuan, Q. Zhu, W.-P. Chen, S. Ling, X. Li, Y.-Z. Zheng, K. Zhu and M. Zhang, *J. Am. Chem. Soc.*, 2020, **142**, 18763–18768; (*e*) J. Dong, Y. Liu and Y. Cui, *Acc. Chem. Res.*, 2021, **54**, 194–206.

4 (*a*) M. D. Ward, C. A. Hunter and N. H. Williams, *Acc. Chem. Res.*, 2018, **51**, 2073–2082; (*b*) A. Galan and P. Ballester, *Chem. Soc. Rev.*, 2016, **45**, 1720–1737; (*c*) H. Amouri, C. Desmarets and J. Moussa, *Chem. Rev.*, 2012, **112**, 2015–2041.

5 (*a*) D. Zhang, T. K. Ronson, Y.-Q. Zou and J. R. Nitschke, *Nat. Rev. Chem*, 2021, **5**, 168–182; (*b*) D. Zhang, T. K. Ronson, R. Lavendomme and J. R. Nitschke, *J. Am. Chem. Soc.*, 2019, **141**, 18949–18953; (*c*) P. C. Purba, M. Maity, S. Bhattacharyya and P. S. Mukherjee, *Angew. Chem., Int. Ed.*, 2021, **60**, 14109–14116; (*d*) D. Chakraborty, R. Saha, J. K. Clegg and P. S. Mukherjee, *Chem. Sci.*, 2022, **13**, 11764–11771.

6 (*a*) R. Saha, B. Mondal and P. S. Mukherjee, *Chem. Rev.*, 2022, **122**, 12244–12307; (*b*) C. J. Brown, F. D. Toste, R. G. Bergman and K. N. Raymond, *Chem. Rev.*, 2015, **115**, 3012–3035; (*c*) Y. Xue, X. Hang, J. Ding, B. Li, R. Zhu, H. Pang and Q. Xu, *Coord. Chem. Rev.*, 2021, **430**, 213656–221378.

7 (*a*) J.-S. Wang, K. Wu, C. Yin, K. Li, Y. Huang, J. Ruan, X. Feng, P. Hu and C.-Y. Su, *Nat. Commun.*, 2020, **11**, 4675–4684; (*b*) Q.-Q. Wang, S. Gonell, S. H. A. M. Leenders, M. Duerr, I. Ivanovic-Burmazovic and J. N. H. Reek, *Nat. Chem.*, 2016, **8**, 225–230.

8 (*a*) L. Zhao, X. Jing, X. Li, X. Guo, L. Zeng, C. He and C. Duan, *Coord. Chem. Rev.*, 2019, **378**, 151–187; (*b*) M. R. Wasielewski, *Acc. Chem. Res.*, 2009, **42**, 1910–1921.

9 (*a*) H. Sunohara, K. Koyamada, H. Takezawa and M. Fujita, *Chem. Commun.*, 2021, **57**, 9300–9930; (*b*) D. M. Daiton, S. R. Ellis, E. M. Nichols, R. A. Mathies, F. D. Toste, R. G. Bergman and K. N. Raymond, *J. Am. Chem. Soc.*, 2015, **137**, 10128–10131; (*c*) A. J. Musser, P. P. Neelakandan, J. M. Richter, H. Mori, R. H. Friend and J. R. Nitschke, *J. Am. Chem. Soc.*, 2017, **139**, 12050–12059.

10 (*a*) Y.-X. Hu, W.-J. Li, P.-P. Jia, X.-Q. Wang, L. Xu and H.-B. Yang, *Adv. Opt. Mater.*, 2020, **8**, 2000265; (*b*) K. Wang, K. Velmurugan, B. Li and X.-Y. Hu, *Chem. Commun.*, 2021, **57**, 13641–13654; (*c*) X.-M. Chen, X. Chen, X.-F. Hou, S. Zhang, D. Chen and Q. Li, *Nanoscale Adv.*, 2023, **5**, 1830–1852.

11 (*a*) M. Hao, G. Sun, M. Zuo, Z. Xu, Y. Chen, X. Y. Hu and L. Wang, *Angew. Chem., Int. Ed.*, 2020, **59**, 10095–10100; (*b*) J.-J. Li, H.-Y. Zhang, X.-Y. Dai, Z.-X. Liu and Y. Liu, *Chem. Commun.*, 2020, **56**, 5949–5952; (*c*) Y. Xia, M. Chen, S. Li, M. Li, X. Li, T. Yi and D. Zhang, *J. Mater. Chem. C*, 2022, **10**, 12332–12337; (*d*) Z. Lian, J. He, L. Liu, Y. Fan, X. Chen and H. Jiang, *Nat. Commun.*, 2023, **14**, 2752–2762; (*e*) P. Sutar, V. M. Suresh, K. Jayaramulu, A. Hazra and T. K. Maji, *Nat. Commun.*, 2018, **9**, 3587–3598.

12 (*a*) K. Acharyya, S. Bhattacharyya, H. Sepehrpour, S. Chakraborty, S. Lu, B. Shi, X. Li, P. S. Mukherjee and P. J. Stang, *J. Am. Chem. Soc.*, 2019, **141**, 14565–14569; (*b*) Y. Li, Y. Dong, L. Cheng, C. Qin, H. Nian, H. Zhang, Y. Yu and L. Cao, *J. Am. Chem. Soc.*, 2019, **141**, 8412–8415; (*c*) L. Xu, Z. Wang, R. Wang, L. Wang, X. He, H. Jiang, H. Tang, D. Cao and B. Z. Tang, *Angew. Chem., Int. Ed.*, 2020, **59**, 9908–9913.

13 (*a*) W.-J. Li, X.-Q. Wang, D.-Y. Zhang, Y.-X. Hu, W.-T. Xu, L. Xu, W. Wang and H.-B. Yang, *Angew. Chem., Int. Ed.*, 2021, **60**, 18761–18768; (*b*) Y.-N. Jing, S.-S. Li, M. Su, H. Bao and W.-M. Wan, *J. Am. Chem. Soc.*, 2019, **141**, 16839–16848.

14 (*a*) D. Zhang, W. Yu, S. Li, Y. Xia, X. Li, Y. Li and T. Yi, *J. Am. Chem. Soc.*, 2021, **143**, 1313–1317; (*b*) Z. Zhang, Z. Zhao, Y. Hou, H. Wang, X. Li, G. He and M. Zhang, *Angew. Chem., Int. Ed.*, 2019, **58**, 8862–8866; (*c*) J. R. Piper, L. Cletheroe, C. G. P. Taylor, A. J. Metherell, J. A. Weinstein, I. V. Sazanovich and M. D. Ward, *Chem. Commun.*, 2017, **53**, 408–411; (*d*) A. Kumar, R. Saha and P. S. Mukherjee, *Chem. Sci.*, 2021, **12**, 5319–5329; (*e*) S. Ahmed, A. Kumar and P. S. Mukherjee, *Chem. Mater.*, 2022, **34**, 9656–9665; (*f*) P.-P. Jia, Y.-X. Hu, Z.-Y. Peng, B. Song, Z.-Y. Zeng, Q.-H. Ling, X. Zhao, L. Xu and H.-B. Yang, *Inorg. Chem.*, 2023, **62**, 1950–1957.

15 D. Li, X. Liu, L. Yang, H. Li, G. Guo, X. Li and C. He, *Chem. Sci.*, 2023, **14**, 2237–2244.

16 (*a*) G. V. Oshovsky, D. N. Reinhoudt and W. Verboom, *Angew. Chem., Int. Ed.*, 2007, **46**, 2366–2393; (*b*) L. L. K. Taylor, I. A. Riddell and M. M. J. Smulders, *Angew. Chem., Int. Ed.*, 2019, **58**, 1280–1307.

17 (*a*) E. G. Percástegui, T. K. Ronson and J. R. Nitschke, *Chem. Rev.*, 2020, **120**, 13480–13544; (*b*) O. Bistri and O. Reinaud, *Org. Biomol. Chem.*, 2015, **13**, 2849–2865.

18 (*a*) P. Mal, B. Breiner, K. Rissanen and J. R. Nitschke, *Science*, 2009, **324**, 1697–1699; (*b*) G. Wu, Y. Chen, S. Fang, L. Tong, L. Shen, C. Ge, Y. Pan, X. Shi and H. Li, *Angew. Chem., Int. Ed.*, 2021, **60**, 16594–16599; (*c*) E. G. Percástegui, J. Mosquera, T. K. Ronson, A. J. Plajer, M. Kieffer and J. R. Nitschke, *Chem. Sci.*, 2019, **10**, 2006–2018; (*d*) P. Howlader, B. Mondal, P. C. Purba, E. Zangrando and P. S. Mukherjee, *J. Am. Chem. Soc.*, 2018, **140**, 7952–7960.

19 (*a*) H. Takezawa, K. Shitozawa and M. Fujita, *Nat. Chem.*, 2020, **12**, 574–578; (*b*) D. H. Leung, D. Fiedler, R. G. Bergman and K. N. Raymond, *Angew. Chem., Int. Ed.*,

Open Access Article. Published on 31 August 2023. Downloaded on 1/18/2026 3:45:56 PM.
This article is licensed under a Creative Commons Attribution-NonCommercial 3.0 Unported Licence.

2004, **43**, 963–966; (*c*) W. Cullen, M. C. Misuraca, C. A. Hunter, N. H. Williams and M. D. Ward, *Nat. Chem.*, 2016, **8**, 231–236.

20 (*a*) W. Cullen, H. Takezawa and M. Fujita, *Angew. Chem., Int. Ed.*, 2019, **58**, 9171–9173; (*b*) L.-X. Cai, S.-C. Li, D.-N. Yan, L.-P. Zhou, F. Guo and Q.-F. Sun, *J. Am. Chem. Soc.*, 2018, **140**, 4869–4876; (*c*) X. Han, C. Guo, C. Xu, L. Shi, B. Liu, Z. Zhang, Q. Bai, B. Song, F. Pan, S. Lu, X. Zhu, H. Wang, X.-Q. Hao, M.-P. Song and X. Li, *ACS Nano*, 2023, **17**, 3723–3736.

21 H. Wang, C. H. Liu, K. Wang, M. Wang, H. Yu, S. Kandapal, R. Brzozowski, B. Xu, M. Wang, P. Eswara, M. P. Nieh, J. Cai and X. Li, *J. Am. Chem. Soc.*, 2019, **141**, 16108–16116.

22 (*a*) J. Mei, N. L. C. Leung, R. T. K. Kwok, J. W. Y. Lam and B. Z. Tang, *Chem. Rev.*, 2015, **115**, 11718–11940; (*b*) X. Yan, T. R. Cook, P. Wang, F. Huang and P. J. Stang, *Nat. Chem.*, 2015, **7**, 342–348; (*c*) X. Yan, M. Wang, T. R. Cook, M. Zhang, M. L. Saha, Z. Zhou, X. Li, F. Huang and P. J. Stang, *J. Am. Chem. Soc.*, 2016, **138**, 4580–4588; (*d*) V. M. Suresh, A. De and T. K. Maji, *Chem. Commun.*, 2015, **51**, 14678–14681.

23 (*a*) S.-D. Wang, C.-L. Lai, Y.-X. Zhang, S.-T. Bao, K.-L. Lv and L.-L. Wen, *J. Mater. Chem. A*, 2022, **10**, 20975–20983; (*b*) M. Forchetta, F. Sabuzi, L. Stella, V. Conte and P. Galloni, *J. Org. Chem.*, 2022, **87**, 14016–14025.

24 (*a*) Y. Zhi, S. Ma, H. Xia, Y. Zhang, Z. Shi, Y. Mu and X. Liu, *Appl. Catal., B*, 2019, **244**, 36–44; (*b*) Y. Cheng, W. Ji, X. Wu, X. Ding, X. Liu and B. Han, *Appl. Catal., B*, 2022, **306**, 121110–121122.

25 (*a*) C.-Q. Ma, X.-L. Li, N. Han, Y. Wang, R.-Z. Wang, S. Yu, Y.-B. Wang and L.-B. Xing, *J. Mater. Chem. A*, 2022, **10**, 16390–16395; (*b*) Y. Wang, C.-Q. Ma, X.-L. Li, R.-Z. Dong, H. Liu, R.-Z. Wang, S. Yu and L.-B. Xing, *J. Mater. Chem. A*, 2023, **11**, 2627–2633.

© 2023 The Author(s). Published by the Royal Society of Chemistry